# Design and performance investigation of a sliding-mode adaptive proportional–integral–derivative control for cable-breakage scenario

Vincenzo Di Paola, Stéphane Caro, Matteo Zoppi

RESEARCH

# Design and performance investigation of a sliding-mode adaptive proportional–integral–derivative control for cable-breakage scenario

**Vincenzo Di Paola · Stéphane Caro · Matteo Zoppi**

Received: 17 March 2024 / Accepted: 25 August 2024 / Published online: 9 September 2024


**Abstract** Controlling a cable-driven parallel robot (CDPR) when a cable breaks is challenging. In this paper, a sliding mode adaptive PID control is designed to ensure a safe guidance of the load when a cable fails. Indeed, regardless when a cable breaks, this control makes it possible enchanting the guidance of the load inside the remaining wrench feasible workspace. In other words, it allows reducing the load oscillation and then increasing the safety of the recovery manoeuvre. Performances are evaluated through simulations by considering a spatial CDPR and comparing the results with a PID control.

**Keywords** Cable-driven robots · Cable failure · Emergency strategy · Adaptive control

**Abbreviations**

| | |
|---|---|
| $F_O\,(O, x, y, z)$ | Inertial frame |
| $m_L$ | Mass of the load $\in \mathbb{R}$ |
| $\mathbf{u}_i$ | Cable direction vector $\in \mathbb{R}^3$ |
| $\boldsymbol{\tau}$ | Cable tensions vector $\in \mathbb{R}^m$ |
| $\mathbf{w}_e$ | External wrench vector $\in \mathbb{R}^3$ |
| $\mathbf{W}$ | Wrench matrix $\in \mathbb{R}^{3\times m}$ |

V. Di Paola (✉) · M. Zoppi
Dipartimento di Ingegneria Meccanica, Energetica, Gestionale e dei Trasporti, Università degli Studi di Genova, Via all'Opera Pia 15, 16143 Genova, Italy
e-mail: vincenzo.dipaola@edu.unige.it

M. Zoppi
e-mail: matteo.zoppi@unige.it

V. Di Paola · S. Caro
École Centrale de Nantes, CNRS, LS2N, UMR6004, Nantes Université, Rue de la Noe 3, 44321 Nantes, France
e-mail: stephane.caro@ls2n.fr

## 1 Introduction

The last few years have seen a real transition in the employment of cable-driven parallel robots (CDPRs) from the academic to the industrial sphere.

The architecture of CDPRs mainly involves the use of cables, driven by electric motors through a system of pulleys, to guide a load. These well-established mechanical devices make CDPRs moderately priced and suitable for high-speed tasks, collaborative operations and also applications that require large workspaces [1].

Recently, the industry has been demanding for collaborative robots. In other words, a lot of effort is now spent in order to enable the robot working safely with the human to perform a task. In this regard, although cables fit perfectly for collaborative purposes, due to their inherent deformability, they are also the source of a major issue when a cable breaks.

The failure of a cable shrinks the wrench feasible workspace (WFW), defined by [2], of the robot. As a consequence, the load suddenly lies outside the WFW and can not be controlled properly. The majority of the works in the literature focus on establishing a strategy for recovering the load to

avoid dangerous collisions with the surrounding environment.

In [3], when the cable breaks, a recovery strategy, which consists in re-planning the load trajectory to bring it to a new equilibrium position within the new WFW, is employed. However, here, it is assumed the possibility to determine when the cable breaks, which, in general, is something unpredictable. Similarly, in [4] a straight-line path motion planning strategy is introduced to guide the load in a safe position inside the workspace. Furthermore, in [5], an after-failure oscillatory trajectory was proposed to steer the end-effector towards a safe landing location, guaranteeing positive and bounded tension limits. In [6] the authors propose a strategy that consists of detecting a cable failure and avoiding any consequent motion of the end-effector. Recently, a fault tolerant control framework relying on an adaptive estimation filter for simultaneous fault detection and diagnosis and task recovery has been introduced in [7].

The occurrence of a cable breakage can harm humans and the environment, hence in [8] the idea is to reduce the kinetic energy of the load while using potential fields to compute cable tensions outside the WFW. Another possibility explored by the same authors [9], consists in reconfiguring the CDPR to restore and enlarge the WFW, thus recovering the control over the load. Again, same authors [10] tries to control the dynamic behavior of the system with remaining cables to prevent further damage, such as collisions with the ground.

Another branch of work regards the computation of the cable tensions distribution. In other words, researchers spent effort in developing the so-called tension distribution algorithms (TDAs) both for normal operating conditions and when a cable fails. In particular, in [11] a methodology, based on the projection of the lost wire tension onto the null space of the Jacobian of the manipulator, is presented. In its subsequent work [12], the corrected cable tension is based on Lagrange multiplier for minimizing the norms of the correctional and overall cable tension, respectively. Another recent contribution is given in [13, 14] where a method to calculate cable forces outside the WFW of a CDPR is presented. Force distributions are obtained based on the concept of distance and with the aim of simplifying the implementation while reducing the numerical cost.

Looking at the global context, together the two classes of the above-mentioned works focus on finding the best recovery strategy and TDAs to govern the load when a cable fails. However, those contributions overlook the control part that could be used to make the system more robust and prepared in this scenario. The importance of a quick reaction by the control station has been pointed out in [15]. To this end, this paper introduces an adaptive control technique in which the PID gains are automatically tuned by exploiting a sliding surface, generally employed with sliding mode control [16, 17]. This solution allows reaching an equilibrium position inside the resulting WFW (i.e. after cable failure), while limiting the load oscillation, without assuming any prior knowledge about when the cable breaks.

This paper is structured as follows. Section 2 recalls the main equations governing the CDPRs. Section 3 reviews the issues in finding a solution for the cable distribution problem when a cable fails. Section 4 describes the control technique used for this work. In Sect. 5, a tracking task where a cable fails for a spatial CDPR is investigated and the SM-APID performances are compared with a PID. Finally, the results are summarized in Sect. 6.

## 2 System modeling

In this section, the main equations and symbols necessary to describe the CDPR are hereby reported, see Fig. 1.

The static or dynamic equilibrium of a load in the space, guided by $m$ cables, is governed by the following equation

$$\mathbf{W}\boldsymbol{\tau} + \mathbf{w}_e = \mathbf{0}, \tag{1}$$

where $\mathbf{w}_e \in \mathbb{R}^3$ is the external wrench, which takes into account also the dynamical actions applied to the platform, while $\boldsymbol{\tau} \in \mathbb{R}^m$ is the cable tensions vector, and the term $\mathbf{W} \in \mathbb{R}^{3\times m}$ is the wrench matrix, which is defined as

$$\mathbf{W} = \begin{pmatrix} \mathbf{u}_1 & \dots & \mathbf{u}_m \end{pmatrix}, \tag{2}$$

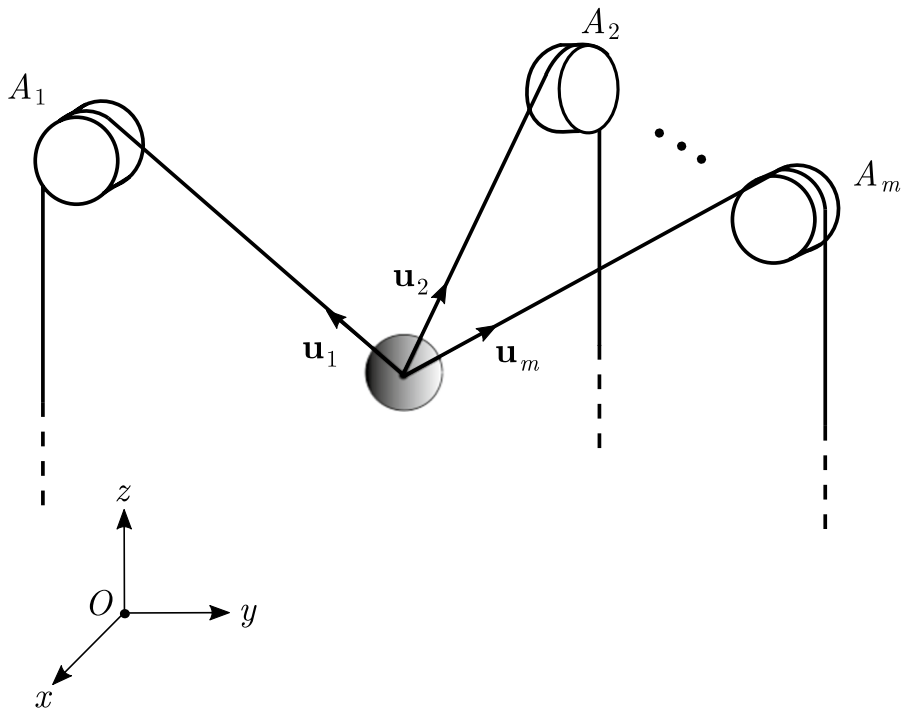


**Fig. 1** CDPR schematic: generic architecture of a cable-driven robot with $m$ cables and a point-mass load

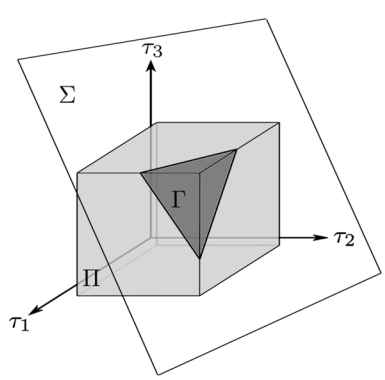


(a) Feasible Solution: graphical representation of $\Pi, \Sigma$ and $\Gamma$ for the case of $m = 3$.

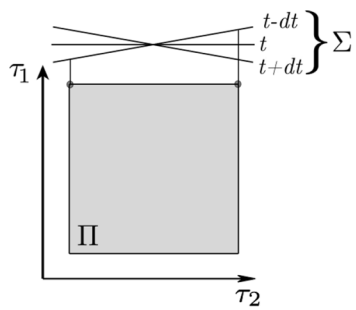


(b) Discontinuity: representation of both the ambiguity at time $t$ and discontinuity of the solution when stepping from time $t - dt$ to $t + dt$ when $m = 2$.

**Fig. 2** Solution properties

here, $\mathbf{u}_i \in \mathbb{R}^3$ represents the *ith* cable direction (unitary vector). Thus, if the Degree of Redundancy[1] (DoR) is greater than one, i.e. $DoR \geq 1$, there exist infinite solutions of Eq. (1) grouped in the following set

$$\Sigma = \left\{ \boldsymbol{\tau} \,|\, \mathbf{W}\boldsymbol{\tau} + \mathbf{w}_e = \mathbf{0} \right\}. \tag{3}$$

However, to maintain the equilibrium of the platform, the cable tension limits have to be taken into account. Hence, the $m$-dimensional convex hypercube $\Pi$ that defines the domain of the *feasible* tensions is

$$\Pi = \left\{ \boldsymbol{\tau} \,|\, \mathbf{0} < \underline{\boldsymbol{\tau}} \leq \boldsymbol{\tau} \leq \overline{\boldsymbol{\tau}} \right\}, \tag{4}$$

where $\underline{\boldsymbol{\tau}}, \overline{\boldsymbol{\tau}} \in \mathbb{R}^{m,+}$ are positive and different tension vectors limits; the tension limits components will be

[1] A redundant CDPR is composed of $m$ cables that exceed the Degree of Freedom (DOF) of the end-effector.

considered equal inside the two vectors, respectively. Consequently, the set of feasible solutions $\Gamma$, see Fig. 2a, satisfying both Eqs. (1) and (4), is

$$\Gamma = \Sigma \cap \Pi. \tag{5}$$

Practically, the cable tensions can be computed as

$$\boldsymbol{\tau} = -\mathbf{W}^{\dagger}\mathbf{w}_e + \mathbf{N}\boldsymbol{\lambda}, \tag{6}$$

where $\mathbf{W}^{\dagger}$ is the Moore–Penrose pseudo-inverse matrix of $\mathbf{W}$, $\mathbf{N} \in \mathbb{R}^{m\times(m-n)}$ contains the vectors that span the kernel of $\mathbf{W}$, $\boldsymbol{\lambda} \in \mathbb{R}^{(m-n)}$ belongs to the polytope $\Lambda$ defined as follows

$$\Lambda := \{\boldsymbol{\lambda} \in \mathbb{R}^{(m-n)} \mid \underline{\boldsymbol{\tau}} \leq -\mathbf{W}^{\dagger}\mathbf{w}_e + \mathbf{N}\boldsymbol{\lambda} \leq \overline{\boldsymbol{\tau}}\}. \tag{7}$$

It turns out that, to cope with the cable intrinsic property guaranteeing the controllability of the platform during the tasks, a natural way to deal with Eq.(6) consists in solving an optimization problem.

## 3 On the TDAs for cable-breakage scenario

So far, several approaches were presented in the literature, [18], to solve the tension distribution problem. Here, the Analytic Centre (AC), presented in [19] and [20], is employed. To motivate the benefit of using this TDA, even in case of cable breakage, this section compares it with the Nearest Corner method, which is specifically developed for cable failure scenarios in a series of papers by [13, 14].

In other words, when the load is outside the WFW then $\Gamma = \emptyset$. Therefore, one can adopt a specific strategy to choose the cable tensions vector $\boldsymbol{\tau}$ in this case. However, one should notice that every technique would always be a fallback solution as it won't respect $\Pi$ and $\Sigma$ contemporarily. Then, this latter will constitute an approximation that has to be compliant with the force boundaries $\Pi$ so that it can be used for control purposes.

In this context, the most immediate idea, as explained in [13, 14], is basically to project the corners of the hypercube $\Pi$ onto the affine space $\Sigma$ and then using weights (accounting for the distance to the corners) to select a tension $\boldsymbol{\tau}$ as the solution. Although this technique has the advantage of not being iterative and can be easily implemented, it still has issues that are not present with the AC.

One practically-relevant issue concerns the continuity of the solution. Similarly as in the Linear Programming (LP) method, [21], when the affine space undertakes a sequence of orientation, such that it becomes parallel to one face of $\Pi$, then the solution is not unique. Moreover, looking at the mentioned sequence of orientation in Fig. 2b, it is evident that one can step from one corner to another of $\Pi$ hence generating a jump (discontinuity) in cable tension profiles.

The second aspect that should be considered, regards the weights used in this method. Indeed, it seems that the weights determining the tension $\boldsymbol{\tau}$ are not bounded. This can cause problems as it can happen that the solution contains components requiring more than the highest (or lowest) tension value. In case the highest tension is selected, this will stress more the remaining cables and can generate a collapse of the overall structure if other cables fail.

As explained in [20], above mentioned issues do not occur when using the AC. Indeed, barrier functions guarantee the continuity of the solutions and automatically avoid selecting cable tensions outside $\Pi$. Notice that other TDAs can be suitable and then used while respecting continuity and returning a solution inside $\Pi$. However, the advantages of using the AC, as pointed out in [20], make it our preferred solution.

**Remark 1** Using an optimization problem somehow translates into reducing the distance between $\Gamma$ and $\Pi$. Indeed, the solver aims at reducing the residual of Eq.(1), while satisfying $\Pi$, as much as possible. Moreover, using AC, one could define a slack variable [19], to mitigate the infeasibility $\Gamma = \emptyset$, similarly as done in [22].

## 4 Sliding-mode adaptive PID

The objective of the control is to ensure that the load is safely (i.e. reducing the risk of undertaking harmful oscillations) stopped in the new WFW, when a cable breaks. Generally, the Sliding Mode (SM) control is used to guide a system under the

effect of disturbances and uncertainties [23]. To avoid the typical chattering[2] of the SM control, the main control command is demanded to an Adaptive PID which is added to the SM part. The fusion of the two will enable controlling the system in presence of external disturbances, limiting the chattering issue.

### 4.1 Control structure

As anticipated above, the control input is split into two terms [23, 24]

$$\mathbf{u} = \mathbf{u}_{PID} + \mathbf{u}_s, \tag{8}$$

where $\mathbf{u}_s$ is the supervisory control that keeps the system state within some defined boundaries, guaranteeing the stability of the dynamical system. The PID exploits a gradient-based adaptation law for updating its gains, providing robustness of the control. The design of both $\mathbf{u}_s$ and $\mathbf{u}_{PID}$ has been defined in [16].

**Remark 2** The action of the control $\mathbf{u}$ takes the role of the external wrench $\mathbf{w}_e$ in Eq. (1) that the cables have to generate to guide the load along the desired trajectory.

### 4.2 Design of the supervisory control

The role of $\mathbf{u}_s$ is to keep the system state inside a designed constraint set

$$\mathfrak{C} = \{\mathbf{x} \in \mathbb{R}^{2n} \,|\, ||\mathbf{x}||_\infty \leq M_\mathbf{x}\}, \tag{9}$$

where $\tilde{\mathbf{x}}, \dot{\tilde{\mathbf{x}}} \in \mathbb{R}^n$ form the system' state $\mathbf{x} = [\tilde{\mathbf{x}}, \dot{\tilde{\mathbf{x}}}]^T \in \mathbb{R}^{2n}$, $M_\mathbf{x}$ is a pre-specified parameter usually chosen such that $M_\mathbf{x} \geq ||\mathbf{y}||_\infty$ with $\mathbf{y} = \left[\tilde{\mathbf{x}}^{des}, \dot{\tilde{\mathbf{x}}}^{des}\right]$ representing the desired state vector.

Its design relies on the stability of the system, which is briefly outlined below. Hence, to asymptotically attain the zero-error condition, the following Lyapunov function candidate is considered

$$V_e = \frac{1}{2}\mathbf{e}^T\mathbf{\Phi}\mathbf{e}, \tag{10}$$

where $\mathbf{e} = [\tilde{\mathbf{e}}, \dot{\tilde{\mathbf{e}}}]^T \in \mathbb{R}^{2n}$ and $\dot{\mathbf{e}} = [\dot{\tilde{\mathbf{e}}}, \ddot{\tilde{\mathbf{e}}}]^T \in \mathbb{R}^{2n}$ are the state error vectors, which are the time derivatives of $\mathbf{e} = \mathbf{y} - \mathbf{x}$. Generally, $\mathbf{\Phi}$ is defined as a positive definite and symmetric matrix that springs out as the solution of the Lyapunov equation [16, 25]

$$\mathbf{A}^T\mathbf{\Phi} + \mathbf{\Phi}\mathbf{A} = -\mathbf{Q}, \tag{11}$$

where the matrix $\mathbf{Q} \in \mathbb{R}^{2n\times 2n}$ is a given, positive definite symmetric matrix, whereas the matrix $\mathbf{A} \in \mathbb{R}^{2n\times 2n}$ pops out by rewriting the error dynamics as

$$\dot{\mathbf{e}} = \mathbf{A}\mathbf{e} + \mathbf{B}(\mathbf{u}^* - \mathbf{u}_{PID} - \mathbf{u}_s), \tag{12}$$

where $\mathbf{u}^*$ is the so-called feedback linearization control whereas $\mathbf{A}$ and $\mathbf{B}$ are the structure matrices

$$\mathbf{A} = \begin{pmatrix} \mathbf{0} & \mathbf{I} \\ -\mathbf{k}_0 & -\mathbf{k}_1 \end{pmatrix} \quad \text{and} \quad \mathbf{B} = \begin{pmatrix} \mathbf{0} \\ g(\mathbf{x}, \dot{\mathbf{x}}) \end{pmatrix}, \tag{13}$$

where $g(\mathbf{x}, \dot{\mathbf{x}})$ is the affine term of dynamical system [25]. Note that $\mathbf{k}_0 \in \mathbb{R}^{n\times n}$ and $\mathbf{k}_1 \in \mathbb{R}^{n\times n}$ are diagonal matrices whose coefficients are chosen such that the roots of the characteristic polynomial, associated with the differential equation $\ddot{\tilde{\mathbf{e}}} + \mathbf{k}_1\dot{\tilde{\mathbf{e}}} + \mathbf{k}_0\tilde{\mathbf{e}} = \mathbf{0}$, belong to the left-half complex plane.

Thus, a classical strategy to reach the desired output is to exercise a control action that strictly decreases $V_e$, which means that $\mathbf{u}_s$ must meet $\dot{V}_e < 0$.

The derivative of the Lyapunov function can be computed as follows [17]

$$\begin{aligned}\dot{V}_e =& \frac{1}{2}(\dot{\mathbf{e}}^T\mathbf{\Phi}\mathbf{e} + \mathbf{e}^T\mathbf{\Phi}\dot{\mathbf{e}}) \leq -\frac{1}{2}\mathbf{e}^T\mathbf{Q}\mathbf{e} + |\mathbf{e}^T\mathbf{\Phi}\mathbf{B}|(|\mathbf{u}^*| + |\mathbf{u}_{PID}|) \\ & - \mathbf{e}^T\mathbf{\Phi}\mathbf{B}\mathbf{u}_s.\end{aligned} \tag{14}$$

Therefore, to satisfy Eq. (14), the supervisory controller can be chosen as

$$\mathbf{u}_s = \operatorname{sgn}(\mathbf{e}^T\mathbf{\Phi}\mathbf{B})(|\mathbf{u}^*| + |\mathbf{u}_{PID}|). \tag{15}$$

With this design, $\mathbf{u}_s$ constantly intervenes in the control process and the presence of the sgn function leads to chattering. Therefore, to adhere with its supervisory definition and to reduce the chattering, the set of constraints $\mathfrak{C}$ is used. In particular, the Indicator function $I_f$ is introduced in the $\mathbf{u}_s$ design as follows

$$\tilde{\mathbf{u}}_s = I_f\,\mathbf{u}_s \quad \text{where} \quad I_f = \begin{cases} 1, & V_e > V_M, \\ 0, & V_e \leq V_M, \end{cases} \tag{16}$$

[2] The chattering is a *switching* phenomena that makes the control action discontinuous, see Fig. 1.7 at Pag. 8 of [23] to better understand.

with

$$V_M = \frac{1}{2}\lambda_{min}(\mathbf{\Phi})(M_{\mathbf{x}} - ||\mathbf{y}||_\infty)^2, \tag{17}$$

where $\lambda_{min}(\mathbf{\Phi})$ is the minimum eigenvalue of the Lyapunov matrix $\mathbf{\Phi}$ [16, 25]. The introduction of the Indicator function completes its design.

### 4.3 PID adaptive laws

The APID is then supposed to steer the system under ordinary conditions (i.e. $V_e \leq V_M$). The adaptation laws are derived with the aim to reach the so-called sliding mode $\mathcal{S} = \mathbf{0}$ (i.e. insensitivity to external disturbances), where $\mathcal{S}$ is the sliding surface defined as in [23]

$$\mathcal{S} = \dot{\tilde{\mathbf{x}}} - \dot{\tilde{\mathbf{x}}}^{des} - \mathbf{k}_1\tilde{\mathbf{e}} - \mathbf{k}_0 \int \tilde{\mathbf{e}}\, dt. \tag{18}$$

To guarantee approaching the sliding mode, the Lyapunov function approach is exploited with a Lyapunov function candidate as

$$V = \frac{1}{2}\mathcal{S}^2. \tag{19}$$

Again, requiring that $\mathcal{S}(t) \to \mathbf{0}$ for $t \to \infty$ coincides with reducing $V$. Consequently, the gradient method is employed to choose the gains which take directions of maximum slope over $V$. Now, the common expression for a PID controller is

$$\mathbf{u}_{PID} = \mathbf{K}_P\tilde{\mathbf{e}} + \mathbf{K}_I \int \tilde{\mathbf{e}}\, dt + \mathbf{K}_D\dot{\tilde{\mathbf{e}}}, \tag{20}$$

using the gradient method and the chain rule, it is possible to obtain the adaptation laws for the control gain matrices $\mathbf{K}_P$, $\mathbf{K}_I$ and $\mathbf{K}_D$

$$\dot{\mathbf{K}}_{P,ii} = -\gamma\frac{\partial\mathcal{S}\dot{\mathcal{S}}}{\partial\mathbf{K}_P} = -\gamma\frac{\partial\mathcal{S}\dot{\mathcal{S}}}{\partial\mathbf{u}_{PID}}\frac{\partial\mathbf{u}_{PID}}{\partial\mathbf{K}_P} = -\gamma\mathcal{S}\tilde{\mathbf{e}}, \tag{21a}$$

$$\dot{\mathbf{K}}_{I,ii} = -\gamma\frac{\partial\mathcal{S}\dot{\mathcal{S}}}{\partial\mathbf{K}_I} = -\gamma\frac{\partial\mathcal{S}\dot{\mathcal{S}}}{\partial\mathbf{u}_{PID}}\frac{\partial\mathbf{u}_{PID}}{\partial\mathbf{K}_I} = -\gamma\mathcal{S}\int\tilde{\mathbf{e}}\, dt, \tag{21b}$$

$$\dot{\mathbf{K}}_{D,ii} = -\gamma\frac{\partial\mathcal{S}\dot{\mathcal{S}}}{\partial\mathbf{K}_D} = -\gamma\frac{\partial\mathcal{S}\dot{\mathcal{S}}}{\partial\mathbf{u}_{PID}}\frac{\partial\mathbf{u}_{PID}}{\partial\mathbf{K}_D} = -\gamma\mathcal{S}\dot{\tilde{\mathbf{e}}}, \tag{21c}$$

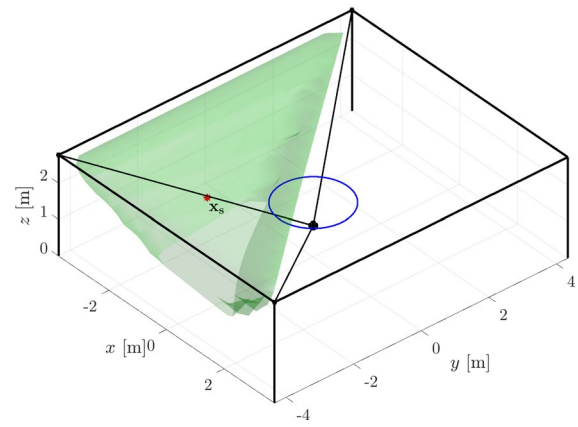


**Fig. 3** WFW: the shape of the WFW is hereby depicted, using the capacity margin [27]. When all the four cables are working, the WFW is symmetric and the trajectory result to be fully inside the green volume. (Color figure online)

where minus is placed opposite to the energy flow $V$ and $\gamma \in \mathbb{R}^+$ is called learning rate.[3]

Hence, the behaviour of the controller can be resumed as follows: if $\mathbf{u}_s = \mathbf{0}$, the PID gains adapt themselves to decrease $V$ to zero (i.e. reach the sliding mode), whereas if $\mathbf{u}_s \neq \mathbf{0}$, the PID gains are not able to decrease $V$ and then also $V_e$ under $V_M$.

**Remark 3** Notice that, when the cable breaks, the load is hardly controllable as the WFW changes. However, the nature of the problem causes the load to sink into the new WFW [3], making it controllable again. From then on, the APID adapts the gains, i.e. it acts actively on the load, in order to reach $\tilde{\mathbf{x}}_s$ while minimising the oscillations or loops around it. Therefore, the change in the WFW can be considered as the presence of uncertainty in the model.

## 5 Study cases

In this section, a CDPR with four cables suspending a point mass load is considered, see Fig. 3 for sake of clarity. The tests consist in tracking a circular and helical trajectory till the cable breaks. When the cable failure occurs, the load is supposed to be positioned

[3] To avoid cumbersome notation, the subscript *ii* (emphasizing the diagonal structure of the gain matrices) has been inserted only to the left-hand side of the equation, intending the derivative operation to be carried out component-wise, [26].

inside the new WFW at the pre-computed *safety* position $\tilde{\mathbf{x}}_s = (-1.2\sqrt{2}, -1.2\sqrt{2}, z(t_{cb}))$[4], while minimizing the kinetic energy by requiring $\dot{\tilde{\mathbf{x}}}_s = (0, 0, 0)$. Observe that one could also combine this procedure by introducing one of the strategy given in the literature; however, this is out of the scope of this paper as the focus is on testing the control part. To simulate this scenario, the integration step is set to $dt = 10^{-3}$ s and it is supposed that the fourth cable is going to fail. This latter does not constitute a loss of generality as indeed, any other cable can be chosen to break by coherently changing the coordinate of $\tilde{\mathbf{x}}_s$ within the new WFW.

Regarding the simulation data, the attachment points are $A_1 = (3.75, -4.34, 2.78)$ m, $A_2 = (-3.75, -4.34, 2.78)$ m, $A_3 = (-3.75, 4.34, 2.78)$ m, $A_4 = (3.75, 4.34, 2.78)$ m, the entire simulations last 20 s, the mass of the load is $m_L = 2$ kg and it is supposed to follow a circular

$$\begin{cases} x(t) = \cos(2\pi s(t)) & s(t) \in [0, 1], \\ y(t) = \sin(2\pi s(t)) & t \in [0, 20] \text{ s}, \\ z(t) = 1.5, \end{cases} \tag{22}$$

or a helical trajectory

$$\begin{cases} x(t) = \sin(\pi/8\, t), \\ y(t) = \cos(\pi/8\, t), \\ z(t) = 1 + 0.05\, t. \end{cases} \tag{23}$$

The gains for the PID are set to be equal to the initial ones of the APID, hence $\mathbf{K}_{P,ii} = \mathbf{K}_{I,ii} = \mathbf{K}_{D,ii} = 10$.

**Remark 4** Literature often reports simulations where, even if a cable breaks, the load remains over-constrained. However, a more significant scenario arises when the load becomes under-constrained after a cable breaks. This would place maximum demands on the controller and enable us to comprehend worst-case performance. Furthermore, notice that considering the suspended architecture makes the case even more challenging since the WFW is not approximated to a cube but to a flipped pyramid and, also, forces along the negative direction of the $z$-axis can not be generated.

[4] Where $z(t_{cb})$ is the z-coordinate recorded at the moment when the cable breaks at a generic time $t_{cb}$.

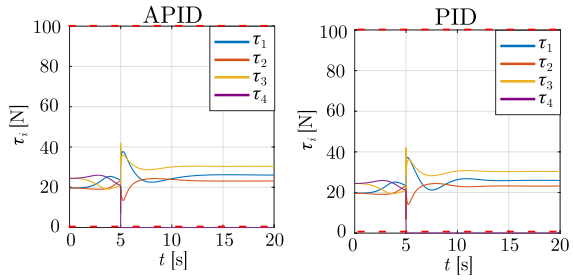


**Fig. 4** Tension profiles: the trend of tension profiles when the fourth cable at $t_{cb} = 5$ s breaks are reported. The tension distribution algorithm used is based on the Analytic centre defined in [20]; dotted red lines identify the cable tension limits. (Color figure online)

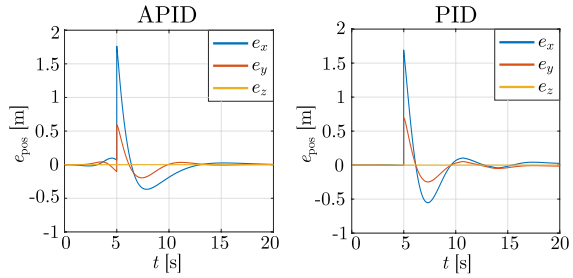


**Fig. 5** distance to the final goal: here the trend of the distance to $\tilde{\mathbf{x}}_s$ recorded, when the cable breaks at $t = 5$ s, along the three Cartesian directions for both the controller PID and APID is represented, respectively

## 5.1 Performances index

This section is placed before the numerical simulations with the scope of introducing a metric to make comparisons between the various control techniques. The index intended to be used here is based on the distance between the load and the safe position. In particular, since the load is expected to oscillate around $\tilde{\mathbf{x}}_s$, the measure of the distance is taken when the load velocity changes its sign. In other words, the position of the load when it inverts its motion $\tilde{\mathbf{x}}_{inv}$ to get $\tilde{\mathbf{x}}_s$ is used for computing the measure. Mathematically the index is defined as

$$\mathcal{I} = ||\tilde{\mathbf{x}}_s - \tilde{\mathbf{x}}_{inv}||, \tag{24}$$

which, merely, represents the maximum radius of the sphere, with centre $\tilde{\mathbf{x}}_s$, within which one can find the load oscillating.

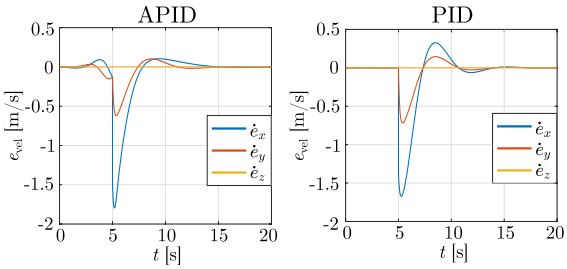


**Fig. 6** Velocity errors: velocity errors recorded when the cable breaks at $t = 5$ s, along the three Cartesian directions for both the controller PID and APID, respectively

## 5.2 Study case one

To start, let's consider the circular trajectory case and set $z(t) = 1.5$ m. Therefore, the tension profiles and the trends of the position and velocity errors for both the PID and APID control are depicted in Figs. 4, 5 and 6, respectively. First, from the error trends, it is possible to see that, when the cable breaks at $t_{cb} = 5$ s, the new $\tilde{\mathbf{x}}_s$ position is automatically defined by the control, and the load is guided toward it. Indeed, at $t_{cb}$ the error suddenly increases since $\tilde{\mathbf{x}}_s$ is generally far from the actual load position. Moreover, it should be evident, comparing the trends, that the use of an adaptive technique makes the system more robust and safer than the PID, as the amplitude of the load oscillations is smaller, see Fig. 5 about 6–13 s. Concerning the convergence to $\tilde{\mathbf{x}}_s$ and $\dot{\tilde{\mathbf{x}}}_s$, from Figs. 5 and 6, it should be clear that the APID performs better as it reaches 0 error before the PID.

A second noteworthy aspect regards the influence of $t_{cb}$ on the control performances. In particular, changing the $t_{cb}$ will help us demonstrate the independence of the APID when the cable fails as well as the robustness of the method.

Therefore, to show what mentioned above, let's consider also cases in which the cable breaks at $t_{cb} = 2.0$ s and $t_{cb} = 3.7$ s. The results of the trajectories followed are depicted in Fig. 7a–c. It seems clear that the PID leads to wider oscillations around $\tilde{\mathbf{x}}_s$ than the APID. The motivation is linked to its fixed gains. Indeed, once selected, they will not be optimal as, in general, the cable breaks unexpectedly.

Comparing the radius $\mathcal{I}_{APID} < \mathcal{I}_{PID}$ only shows the superiority of the APID in guaranteeing safety around a chosen $\tilde{\mathbf{x}}_s$. To show its independence from time, one should notice that the radius under which

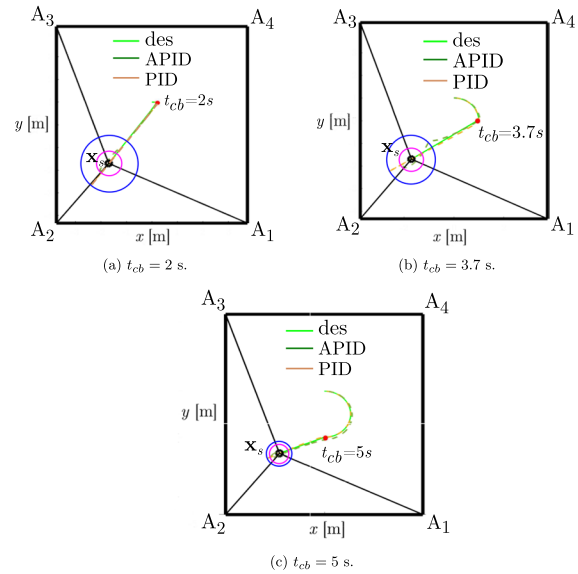


(a) $t_{cb} = 2$ s. (b) $t_{cb} = 3.7$ s. (c) $t_{cb} = 5$ s.

**Fig. 7** Multi-failure scenario: tracked trajectories for different cable-breakage times $t_{cb} = 2$ s, $t_{cb} = 3.7$ s and $t_{cb} = 5$ s for both PID and APID controls. Note the circles highlights the differences in distances between the two methods blue for the PID and purple for the APID. In general, the PID leads to larger oscillations around the safe position $\tilde{\mathbf{x}}_s$ w.r.t. the APID. (Color figure online)

the load oscillates is always smaller than the one defined by the constraint $\mathfrak{C}$ in Eq. 9. In other words, $\mathfrak{C}$ traces a sphere, inside which the load should stay by adapting the gains. If this condition can not be satisfied, then the $\mathbf{u}_s$ intervenes as said at the end of Sec. 4. Notice that the definition of $\mathfrak{C}$ depends on the scalar value $M_{\mathbf{x}}$ which, indeed, is independent from the time. Moreover, one should observe that the radius of the circle $\mathcal{I}_{PID}$ decreases while going from $t_{cb} = 2$ s to $t_{cb} = 5$ s. In other words, the higher the time $t_{cb}$, the lower the radius. This can be explained by observing that, for this case study, the distance to $\tilde{\mathbf{x}}_s$ reduces when $t_{cb}$ increases. Therefore, since the distance reduces, the amount of time where the motion of the load is uncontrolled reduces and then the PID should correct the trajectory less to reduce the error.

**Remark 5** Practically, the parameter $M_{\mathbf{x}}$, as defined in Sec. 4, translates in requiring a certain level of safety by posing limits on $\mathcal{I}$. Clearly, $M_{\mathbf{x}} = 0$ means that the load must stop at $\tilde{\mathbf{x}}_s$ and no oscillations are permitted.

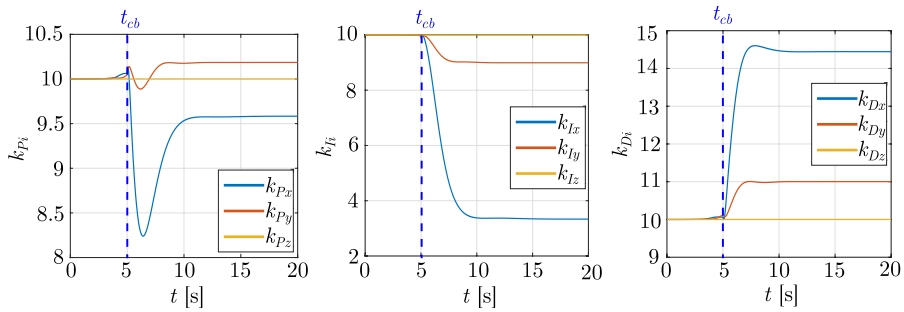


**Fig. 8** Gain trends: gain profiles over time for the APID. Observe that, when the cable breaks at $t_{cb}$, there is a phase of transition before the gains stabilize again. The extremes of this transitional phase are $t_{cb}$ and the instant of time when the load enters the new WFW

For sake of completeness, the gains profiles, Fig. 8, are also reported to show how they change over time. Observe that these graphs tell us when the load enters the new WFW. Indeed, this happens when the gains stabilize at a steady value.

The analysis can be concluded by considering the influence of $\gamma$ on the APID performance. Here, $\gamma$ has been considered fixed to $\gamma = 0.005$ in order to make fair comparisons with the PID. However, several possibilities are available. One can, for example, have different values along each Cartesian direction. Now, despite the broad range of possibilities one has for choosing $\gamma$, practically, its influence on the global behaviour of the control is what interests us for designing the control. In this context, it appears clear that, when $\gamma \to 0$, then the APID behaves as the PID. Therefore, one can think that the higher is $\gamma$ the better it is in terms of adaptation and then performance. This latter conclusion is, however, wrong. Indeed, increasing $\gamma$ can lead to overreaction to errors change, see Eqs. (21a)–(21c). Practically speaking, this last phenomena is not a problem as far as the variation in the gains does not result in actuation saturation. Therefore, it is necessary to find a good compromise between the reaction to error change and the quickness of adaptation.

## 5.3 Study case two

In this section, the trajectory is considered as a helix in order to show the generality of the method and see if major changes in the result occur.

Similarly to what was done before, let us analyse the performance of both the PID and APID when the fourth cable breaks. For brevity, only the case $t_{cb} = 2$ s is reported as it is the worst case due to the large distance separating the point where the cable breaks and the $\tilde{\mathbf{x}}_s$.

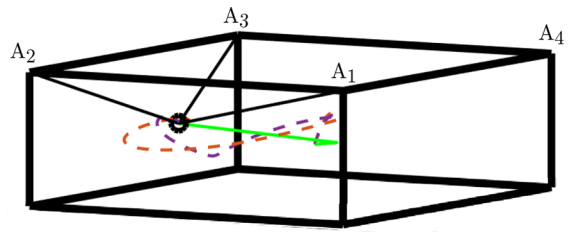


**Fig. 9** Simulation results: this figure represents the trajectories undertaken by the load when a cable breaks. In particular the red curve is obtained with the PID whereas the purple with the APID control. Notice that the green represents the ideal trajectory to be followed when the cable braks. (Color figure online)

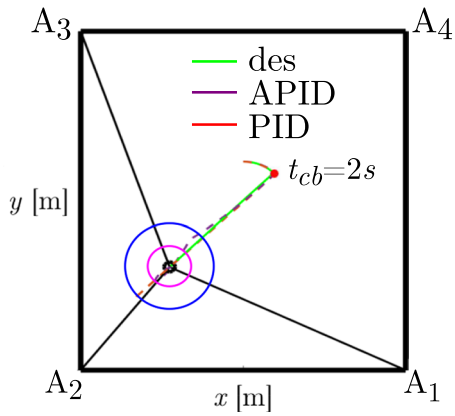


**Fig. 10** PID control

Qualitatively comparing the trajectories undertaken by the load in Figs. 9 and 10 suffices to confirm what said before $\mathcal{I}_{APID} < \mathcal{I}_{PID}$.

One additional information that can be added by looking at the spatial trajectory in Fig. 9 regards the radius of the sphere around the safe position.

In previous simulations, the error in the $z$ direction was small (about 0) and then there was no doubt about taking the radius as the maximum distance on the $x-y$ plane. This time, one can argue that this consideration is not valid anymore. However, since typically the aim is to avoid lateral collisions first, it should be still valid taking the radius as the maximum on the $x-y$ plane as safety criteria to compare the control performance.

## 6 Conclusion

Motivated by the question of whether a control technique could assist in controlling the load in the case of cable failure rather than using lock-in strategies, in this paper, the performance of the SM-APID was investigated. The proposed control guarantees a higher robustness w.r.t. the well-known PID method, which has fixed gains and then no flexibility in terms of responsiveness. Indeed, the obtained results served as motivation for integrating gain adaptation laws on CDPRs to make them more robust when unpredictable phenomena occur to destabilize the load. The experimental validation of this technique will be part of the future works.

**Author contributions** V.D.P. has taken the lead as the primary author, spearheading the definition of simulations, creating visual representations, and drafting significant portions of the written content. S.C. and M.Z. thoroughly reviewed the manuscript, providing valuable insights and suggestions to enhance its scientific consistency, clarity, and reproducibility.

**Funding** Open access funding provided by Università degli Studi di Genova within the CRUI-CARE Agreement.

**Data availability** No datasets were generated or analysed during the current study.

**Declaration**

**Conflict of interest** The authors declare no Conflict of interest.



## References

1. Bruckmann T, Pott A (2018) Cable-driven parallel robots. Springer tracts in advanced robotics. Springer, Cham. https://doi.org/10.1007/978-3-319-76138-1
2. Bouchard S, Gosselin C, Moore B (2010) On the ability of a cable-driven robot to generate a prescribed set of wrenches. J Mech Robot. https://doi.org/10.1115/1.4000558
3. Berti A, Gouttefarde M, Carricato M (2016) Dynamic recovery of cable-suspended parallel robots after a cable failure. In: Advances in Robot Kinematics 2016. Springer, Cham. https://doi.org/10.1007/978-3-319-56802-7-35
4. Boschetti G, Passarini C, Trevisani A (2017) A strategy for moving cable driven robots safely in case of cable failure. In: Advances in Italian mechanism science: proceedings of the first international conference of IFToMM Italy. https://doi.org/10.1007/978-3-319-48375-7-22
5. Passarini C, Zanotto D, Boschetti G (2019) Dynamic trajectory planning for failure recovery in cable-suspended camera systems. J Mech Robot. https://doi.org/10.1115/1.4041942
6. Boschetti G, Carbone L, Passarini C (2019) Cable failure operation strategy for a rehabilitation cable-driven robot. Robotics. https://doi.org/10.3390/robotics8010017
7. Raman A, Walker I, Krovi V, Schmid M (2023) Cable failure tolerant control and planning in a planar reconfigurable cable driven parallel robot. Front Robot AI. https://doi.org/10.3389/frobt.2023.1070627
8. Boumann R, Bruckmann T (2019) Development of emergency strategies for cable-driven parallel robots after a cable break. Springer International Publishing, Cable-Driven Parallel Robots. https://doi.org/10.1007/978-3-030-20751-9-23
9. Boumann R, Bruckmann T (2021) An emergency strategy for cable failure in reconfigurable cable robots. Springer International Publishing, Cable-Driven Parallel Robots. https://doi.org/10.1007/978-3-030-75789-2-18
10. Boumann R, Bruckmann T (2022) Simulation and model-based verification of an emergency strategy for cable failure in cable robots. Robotics. https://doi.org/10.3390/act11020056
11. Notash L (2012) Failure recovery for wrench capability of wire-actuated parallel manipulators. Robotica. https://doi.org/10.1017/S0263574711001160
12. Notash L (2013) Wrench recovery for wire-actuated parallel manipulators. In: Padois V, Bidaud P, Khatib O (eds) Robot design, dynamics and control (ROMANSY),

CISM. Springer, Vienna. https://doi.org/10.1007/978-3-7091-1379-0-25
13. Boumann R, Bruckmann T (2020) Computationally efficient cable force calculation outside the wrench-feasible workspace. In: Robotics and mechatronics. Springer International Publishing, Cham. https://doi.org/10.1007/978-3-030-30036-4-15
14. Boumann R, Bruckmann T (2020) Real-time cable force calculation beyond the wrench-feasible workspace. Robotics. https://doi.org/10.3390/robotics9020041
15. Boschetti G, Minto R, Trevisani A (2021) Experimental investigation of a cable robot recovery strategy. Robotics. https://doi.org/10.3390/robotics10010035
16. Chang W-D, Yan J-J (2005) Adaptive robust PID controller design based on a sliding mode for uncertain chaotic systems. Chaos Solitons Fractals. https://doi.org/10.1016/j.chaos.2004.12.013
17. Di Paola V, Goldsztejn A, Zoppi M, Caro S (2023) Design of a sliding mode-adaptive PID control for aerial systems with a suspended load exposed to wind gusts. J Comput Nonlinear Dyn. https://doi.org/10.1115/1.4062324
18. Pott A, Bruckmann T, Mikelsons L (2009) Closed-form force distribution for parallel wire robots. In: Kecskeméthy A, Müller A (eds) Computational kinematics. Springer, Berlin, Heidelberg. https://doi.org/10.1007/978-3-642-01947-0-4
19. Ueland E, Sauder T, Skjetne R (2020) Optimal force allocation for overconstrained cable-driven parallel robots: continuously differentiable solutions with assessment of computational efficiency. IEEE Trans Robot. https://doi.org/10.1109/TRO.2020.3020747
20. Di Paola V, Goldsztejn A, Zoppi M, Caro S (2024) Analytic center based tension distribution for cable-driven platforms (CDPs). J Mech Robot (JMR). https://doi.org/10.1115/1.4065244
21. Borgstrom PH, Jordan BL, Sukhatme GS, Batalin MA, Kaiser WJ (2009) Rapid computation of optimally safe tension distributions for parallel cable-driven robots. IEEE Trans Rob. https://doi.org/10.1109/TRO.2009.2032957
22. Côté AF, Cardou P, Gosselin C (2016) A tension distribution algorithm for cable-driven parallel robots operating beyond their wrench-feasible workspace. In: 16th international conference on control, automation and systems (ICCAS). https://doi.org/10.1109/ICCAS.2016.7832301
23. Yuri S, Christopher E, Leonid F, Arie L (2014) Sliding mode control and observation. Springer, New York. https://doi.org/10.1007/978-0-8176-4893-0
24. Hsueh Y-C, Su S-F (2007) Supervisory controller design based on Lyapunov stable theory. In: 2007 IEEE international conference on systems, man and cybernetics. https://doi.org/10.1109/ICSMC.2007.4413948
25. Zabczyk J (2020) Mathematical control theory, an introduction. Springer, Cham. https://doi.org/10.1007/978-3-030-44778-6
26. Noordin A, Mohd Basri MA, Mohamed Z, Mat Lazim I (2021) Adaptive PID controller using sliding mode control approaches for quadrotor UAV attitude and position stabilization. Arab J Sci Eng. https://doi.org/10.1007/s13369-020-04742-w
27. Ruiz ALC, Caro S, Cardou P, Guay F (2015) Arachnis: analysis of robots actuated by cables with handy and neat interface software. In: 2nd international conference on cable-driven parallel robots